Electrical activity and migration of 90 degrees partial dislocations in SiC

Article (Published Version)

Electrical activity and migration of 90° partial dislocations in SiC

New Journal of Physics
The open–access journal for physics

Electrical activity and migration of 90° partial dislocations in SiC

G Savini[1,4], M I Heggie[1], S Öberg[2] and P R Briddon[3]

[1] Department of Chemistry, University of Sussex, Brighton BN1 9QJ, UK
[2] Department of Mathematics, University of Luleå, SE-97187, Luleå, Sweden
[3] School of Natural Sciences, University of Newcastle upon Tyne, Newcastle upon Tyne, NE1 7RU, UK
E-mail: g.savini@sussex.ac.uk

New Journal of Physics **9** (2007) 6
Received 12 September 2006
Published 17 January 2007
Online at http://www.njp.org/
doi:10.1088/1367-2630/9/1/006

Abstract. SiC *p-i-n* diodes exhibit an increase in the voltage drop under forward bias which has been linked with the increased mobility of partial dislocations. Through first-principles calculations, we investigated the Si(g) and C(g) core 90° partials in 4H-SiC. We showed that both dislocations can sustain the asymmetric and symmetric reconstructions along the dislocation line. The latter reconstructions are always electrically active with a half-filled metallic band and are always more likely to migrate with substantially lower activation energies. Further we have suggested that under forward bias, the 90° partials are less mobile than the 30° partial dislocations.

[4] Author to whom any correspondence should be addressed.

PII: S1367-2630(07)32505-6

Contents

1. Introduction

Silicon carbide is a very promising material for high-power, high-temperature and high-frequency applications. In comparison with the other semiconductor materials, silicon carbide distinguishes itself by a combination of superior properties, such as high thermal conductivity, high thermal stability, high critical breakdown field, hardness second to diamond and high resistance to radiation. This semiconductor can exist in more than 200 polytype structures with a wide band gap ranging from 2.3 eV for the 3C–SiC to 3.3 eV for the 4H-SiC polytype [1].

Despite its outstanding properties, recent experiments have shown that *p-i-n* diodes rapidly degrade under electrical injection of carriers [2]. Such behaviour renders the SiC diodes much less attractive than they could potentially be. For example, high-power systems are frequently designed with several diodes connected in parallel in order to increase the total current rating. The increase in the resistance of one diode due to degradation processes would increase the current flow in the remaining stable components. At some point, the current flowing through the stable diodes could exceed the threshold maximum current of the devices and the system could fail catastrophically.

This degradation process is due to enhancement of the partial dislocation mobility followed by an expansion of Shockley stacking fault in the active region of the device [3, 4]. Among all the possible types of partial dislocations, only two are observed during the degradation process, the 30° carbon core (C(g) 30° partial) and the 30° silicon core (Si(g) 30° partial). Several studies using different experimental techniques with different sample orientations have shown that only the Si(g) core moves rapidly, while the C(g) core is almost immobile [5]–[7]. Further, a near-band-gap transition is observed at approximately 1.8 eV associated with the 30° partials which border the growing stacking faults [3].

The drastic lowering of the glide activation energy (by about ten times) is due to the recombination-enhanced dislocation glide (REDG). According to this phonon-kick mechanism, a recombination centre should be present along the dislocation line and the released transition energy transferred into the reaction coordinate for glide migration of the Shockley partials [8]–[10]. It is important to stress that the REDG mechanism always requires a deep level localized along the dislocation line.

As in silicon and diamond, the 90° partials with double-period have slightly lower energy than the single-period structures (by about 90–100 meV Å^{-1} [11]). The double period possesses two types of reconstruction bonds between like atoms, one of which lies in the faulted region and the other type in the unfaulted region. However, both double and single period have nearly identical bond lengths and similar energies are expected for kink migrations [11]. Theoretical studies have shown that the activation energy for the kink migrations of partial dislocations ranges from 2.3 eV for the C(g) core 90° partials to 4.1 eV for the Si(g) core 30° partials. In both the 90° and 30° dislocations, only the Si(g) core partials are electrically active with a corresponding band-gap level at $E_v + 0.4$ eV [11]. So far, the origins of the deep level required by the REDG process and the 1.8 eV radiative transitions related to the partial dislocations remain unexplained.

At present it is not clear why the 90° partials are not observed during the degradation process and two possible scenarios are likely. In the first one, the glide activation energies of the 90° partials could be much higher than the 30° partials, thus only stacking fault bounded by 30° partial segments nucleate and expand under forward bias. In the second scenario, the glide activation energies of 90° partials could be much lower than the 30° partials; as a result the 90° partials should disappear, leaving only the 30° partials in the crystal [12].

The aim of our work is to study the symmetric reconstructions (SRs) of 90° partials and whether these reconstructions can enhance the dislocation velocity. We have shown that these reconstructions characterized by dangling bonds along the dislocation line are always electrically active (as required by the REDG mechanism) and have glide activation energies substantially lower than the asymmetric reconstructions (ARs). However in order to stabilize the SRs, a shear between the unfaulted and stacking fault regions at the core of the partials is required. Since the 30° partials should not require a long ranged shear, we have suggested that under forward bias, the glide activation energies of the 90° partial dislocations are higher than the 30° partial dislocations.

2. Computational methods

Ab initio calculations have been performed within the density functional theory (DFT). The exchange-correlation energy has been determined using the local density approximation with the functional as parameterized by Perdew and Wang [13]. The employed wavefunction basis sets consist of s, p and d Gaussian orbital functions with four exponents centred at the atomic sites [14]. Norm-conserving pseudopotentials based on the Hartwigsen–Goedecker–Hutter scheme are used [15], while the charge density is expanded in plane waves up to 300 Ryd.

To perform the Brillouin zone (BZ) integrations, we used the Monkhorst–Pack (MP) scheme [16] with eight k-points along the dislocation line. In order to take into account the possible dispersion of the levels inside the band-gap, a metallic filling is used, where the number of electrons at each k-point can differ. The initial atomic positions have been produced with isotropic elastic theory, then relaxed using DFT and the conjugate gradient algorithm.

3. Dislocation core structures

In hexagonal SiC the partial dislocations lie in the basal plane with Burgers vector $\mathbf{b_p} = \frac{1}{3}[10\bar{1}0]$ and the dislocation line along $\mathbf{l} = [1\bar{2}10]$. To model the dislocations, we used a supercell-cluster hybrid approach. In this model, the periodicity of the lattice is kept only along the dislocation

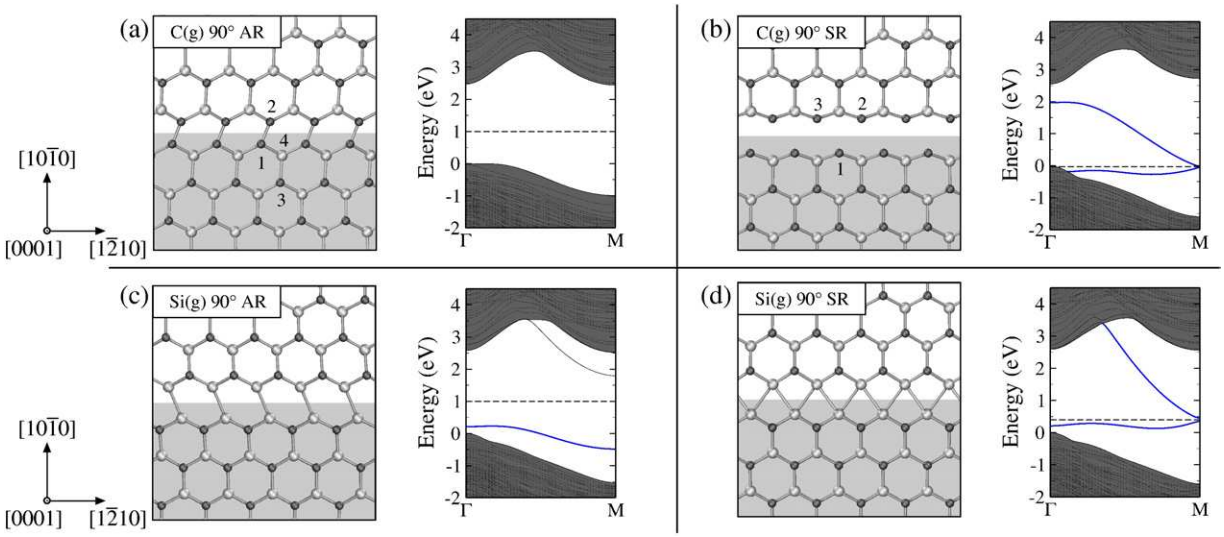

Figure 1. Projections on the glide plane [0001] of the partial dislocations and the respective Kohn–Sham band structures in the neutral charge states. Left panel: AR; right panel: SR; Top panel: the C(g) core 90° partial dislocations; bottom panel: the Si(g) core 90° partial dislocations; The intrinsic stacking fault regions accompanying the partials are shaded. The Fermi level separating occupied and unoccupied states is indicated by a dashed line.

line (supercell component), while within the plane the unit cell is repeated keeping an empty space between the cluster and its images in the neighbouring unit cells of $\Delta = 8$ au (cluster component). The silicon and carbon bonds along the surface are saturated by hydrogen like atoms. The stoichiometries of unit cells are $Si_{84}C_{84}H_{52}$ for a total of 220 host atoms. The possible reconstructions along the dislocation line are shown in the figure 1. The SRs are characterized by dangling bonds (or quasi-5-fold bonded atoms) along the dislocation line. In the ARs atoms in pairs form bonds along the dislocation line. The atomic structures and the respective band structures depicted in figure 1 refer to the neutral charge states.

Depending on the position of the Fermi level in the bulk band gap, both the partials can sustain the AR and SR reconstructions along the dislocation line. The formation energies of the respective reconstructions in the different charge states are defined by [17]

$$E^q_{\text{form}} = E^q_{\text{tot}} - E_{\text{bulk}} + q[E_{\text{F}} + E_{\text{v}} + \Delta V], \tag{1}$$

where E^q_{form} is the formation energy of the dislocation in the q charge state, E^q_{tot} is the total energy of the unit cell containing a dislocation with charge q, E_{bulk} is the energy of the bulk with the same stoichiometry and E_{F} is the Fermi energy with respect to the top of the valence band (VB) E_{v}. The potential ΔV is a correction term in order to line up the band structures of the different charge states with the bulk [18]. The Coulomb divergences of charged supercells are circumvented by a cancelling uniform charge density of opposite sign (the so-called jellium background charge). Test calculations have shown that the formation energies of 110 and 220 host atom unit cells are consistent therefore no attempts are made to correct the electrostatic interactions between neighbouring charged unit cells.

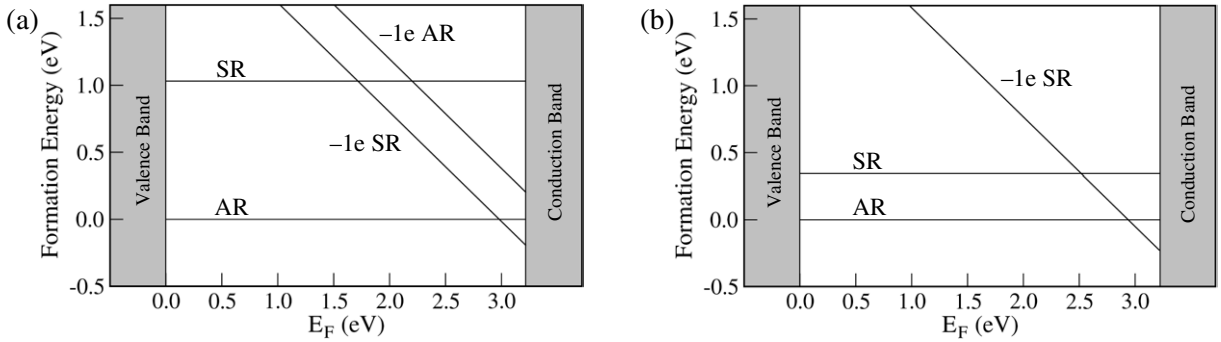

Figure 2. Formation energy as a function of the Fermi level for the neutral and negative core reconstructions. (a) C(g) core dislocations; (b) Si(g) core dislocations. The lowest formation energy segments are the stable reconstructions. For the Si(g) core partial the negative charge state AR is not stable and turns automatically into the SR one.

The formation energies as a function of the Fermi level of the most stable charge states are shown in figure 2. In general we found that the AR is always favourable in p-doped and intrinsic bulk, while the SR may become stable in strongly n-type material. In the SR the dangling bonds, which are always present along the dislocation line, give rise to a half-filled band (see figure 1). The AR is characterized by strong covalent bonds which split the half-filled band generating a fully occupied band near the top or inside the bulk VB and an unoccupied band in the conduction band (CB). In figure 1, the electronic states under or above the Fermi level are fully occupied or empty levels, respectively.

Figure 3 shows the formation energy of the C(g) core dislocation versus the lengths between like atoms along the dislocation line for the neutral and negative charge state $-1e$/per repeat distance along the dislocation line (3.06 Å). To investigate the transition between the AR and the SR core structures, we define the following constraint

$$c_{\text{core}} = |R_1 - R_2|^2 - |R_1 - R_3|^2, \tag{2}$$

where R indicates the atomic coordinates and the subscript denotes the atom number as depicted in figure 1(b). In case of the SR the constraint c_{core} is zero, reflecting the equal distance between like atoms along the dislocation line (see figure 1(b) and (d)). For the AR the constraint c_{core} is negative or positive depending on the possible orientations of the reconstruction bonds along the dislocation line (the constraint is positive for figure 1(a) and negative for figure 1(c)).

For the neutral charge dislocations (solid line in figure 3), the AR is always energetically favourable with respect to the SR by about 1.03 eV per repeat distance for the C(g) core and 0.34 eV per repeat distance for the Si(g) core dislocation, while the SR is a saddle point between the two possible orientations of the reconstruction bonds.

For the negative charge state the C(g) core AR becomes a metastable structure (i.e. local minimum) with respect to the SR with a difference in formation energies of about 0.39 eV per repeat distance, while the Si(g) core AR becomes unstable turning into the SR core structure spontaneously. We observed that the SR requires a shear between the unfaulted and stacking fault regions along the dislocation line of the AR. The latter shear ranges between 0.8–1.2 Å for the C(g) core and 1.0–1.3 Å for the Si(g) core partials. In the following discussion, we describe

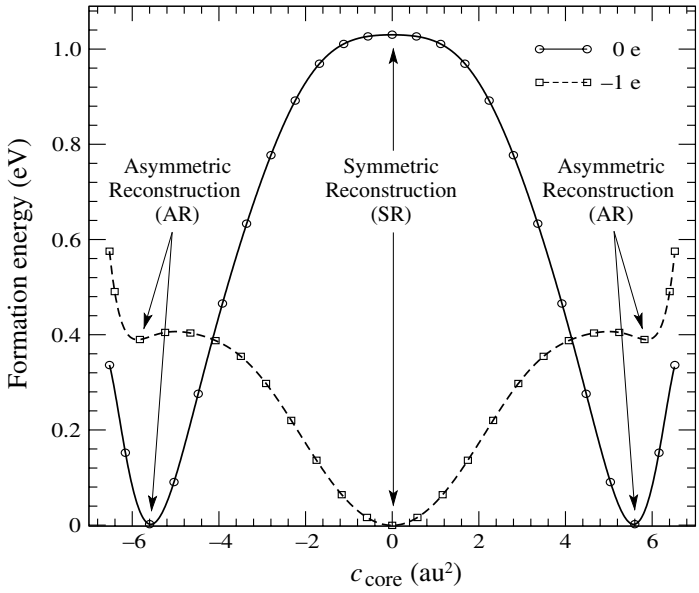

Figure 3. Formation energy for the C(g) core dislocation versus distance between like atoms along the dislocation line. In neutral charge state, the AR is energetically favourable (solid line) and the SR is a saddle point. In the negative charge state, the SR is favourable while the AR is a metastable structure (dashed line). The energies of the two stable structures are set to be coincident.

in detail the respective core structures and electrical properties of both the partials. When we describe the negative charge state, we are always referring to charge state $-1e$ per repeat distance (3.06 Å).

3.1. C(g) core dislocations

In *p*-doped and intrinsic bulk, the AR is always favourable. The C–C bond length is 1.65 Å, while the C–Si back bonds of the core atoms range in length from −3.2 to 5.5% compared with the bulk SiC. This reconstruction is not electrically active. In strongly *n*-type doping, the SR may become more stable. In the neutral charge state, the dangling bonds along the dislocation line are separated by 2.56 Å, expanded by 67% from the bulk diamond bond length. As a consequence, the back bonds of 3-fold coordinate core atoms are shortened (by ∼2.6%). The dangling bonds localized on the C atoms give rise to a half-filled band ranging from inside the VB to $E_{\mathrm{v}} + 1.97$ eV. In the negative charge state the distance between dangling bond atoms is 2.69 Å, 5.1% longer than the respective neutral charge state, while the back bonds of the C atoms are shortened by 5.1% with respect to the bulk SiC. The band structure analysis shows a deep band ranging from $E_{\mathrm{v}} + 0.06$ eV to inside the CB.

3.2. Si(g) core dislocations

Again in *p*-doped and intrinsic bulk the AR is always favourable. The Si–Si bond length is 2.38 Å, while the back bonds are distorted by ±1.6%. The band structure analysis gives a donor level $E_{\mathrm{v}} + 0.21$ eV at the Γ-point and opens a little gap at the boundary of the BZ. In heavily *n*-type

Table 1. Band-gap levels at the Γ-point of the BZ in the neutral charge states. Both the SRs are electrically active with a deep band across the forbidden band-gap

Dislocation	AR	SR
C(g) core	—	$E_v + 1.97\,eV$
Si(g) core	$E_v + 0.21\,eV$	$E_v + 0.21\,eV$

doped material, the SR may become favourable. In the neutral charge state the Si atoms along the dislocation line are quasi 5-fold coordinate with a bond length of 2.69 Å, expanded by 15.0% with respect to the bulk silicon. The back bonds of the Si core atoms range between −1.0 and 0.4% compared to the bulk SiC. The band structure analysis shows a half-filled band ranging from $E_v + 0.21$ eV to inside the CB. In the negative charge state the bond lengths between like atoms along the dislocation line are 2.58 Å, 4% smaller than the neutral state. The back bonds are slightly shortened (by ∼1.9%) with respect to the bulk SiC. The band structure analysis shows a deep band ranging from $E_v + 0.38$ eV to inside the CB.

In conclusion, for the AR only the Si(g) core partials give rise to a narrow band at $E_v + 0.2$ eV in substantial agreement with what was found previously ($E_v + 0.40$ eV [11]). The small difference between the two values can be attributed to the different sizes of the unit cell: 120 host atoms with 1 × 1 × 2 MP set of k-points in [11], against 220 atoms with 1 × 1 × 8 MP grid in the present study. In the SR both the partials are electrically active with a half-filled deep band (see table 1). In the following two sections, we describe the mobility of the AR and SR reconstructions in their more stable charge states, i.e. the neutral charge state for the ARs and the negative charge state for the SRs. In this way, the reconstructions under investigation are always the global minimum energy reconstructions.

4. Peierls barrier of the first kind

The nature of the resistance to dislocation glide is either intrinsic or extrinsic [19]. The intrinsic component is the resistance of a dislocation in a perfect crystal (lattice friction), while the extrinsic resistance is due to defects and impurities always present in a real crystal. The amount of decoration of a dislocation by defects will depend on the history of the sample. Heavily dislocated or networked material will suffer enormously from this problem. However, the SiC substrates are generally carefully grown rather pure and undeformed, so these effects are less likely. In addition, decorated dislocations are usually pinned, i.e. point defects decrease the dislocation mobility, but freshly produced dislocations can glide and, in gliding, dislocations discard point-defect atmospheres (the so-called Cottrell atmosphere). Therefore, we consider it appropriate to discuss the mobility of clean stoichiometric glide dislocations, where the resistance to the dislocation glide (the intrinsic component) is due to the Peierls potential which reflects the discreteness of the crystalline lattice [20].

The elementary processes of dislocation migration controlled by the Peierls mechanism consist of kink pair formation and the subsequent migration of kinks along the dislocation line.

Table 2. Peierls barrier of the first kind for both the ARs and SRs in each favourable charge state.

	Core structure	$Q_{\text{first kind}}$ (eV)
C(g) core	AR (0 e)	1.71
	SR (-1 e)	0.42
Si(g) core	AR (0 e)	2.01
	SR (-1 e)	1.84

The dislocation velocity v_{dis} is given by

$$v_{\text{dis}} \propto \mathrm{e}^{-\frac{Q-TS}{kT}}, \tag{3}$$

where Q is the activation energy and S is an entropy term. We have first calculated the Peierls barrier of the first kind where the dislocation line moves rigidly across the Peierls valley. These barriers are an approximation as the dislocation migrations always follow the kink pair formation and the subsequent migration of kinks. Nevertheless this study could give reliable results inasmuch as the kink migration energy (Peierls potential of the second kind) is lower than the kink pair formation energy (Peierls potential of the first kind). The former case is called the smooth kink regime in which the time spent by the kink migration over the whole dislocation segment is much shorter than the average time of kink pair formation and the dislocation velocity is determined solely by the frequency of the kink pair formation. Whereas in the case of abrupt kink regime the kink migration energy is higher than the kink pair formation energy and the dislocation velocity is controlled by both kink pair formation rate and kink migration velocity.

The stoichiometries of unit cells are $Si_{42}C_{42}H_{26}$ for a total of 110 host atoms. To investigate the intermediate structures between the initial and migrated dislocations, we have calculated the energy surface of 10×10 intermediate points defined by the following constraints

$$c_{\text{silicon}} = |R_1 - R_2|^2 - |R_1 - R_3|^2; \quad c_{\text{carbon}} = |R_4 - R_3|^2 - |R_4 - R_2|^2, \tag{4}$$

where R represents the atomic coordinates and the subscripts are the atomic numbers as depicted in figure 1(a).

The Peierls barriers of the first kind for each of the core reconstructions are given in table 2. The Peierls barrier for the C(g) core partials is lowered from 1.71 eV for the AR to 0.42 eV for the SR, while for the Si(g) core dislocations, the respective Peierls barrier is lowered from 2.01 eV for the AR to 1.84 eV for the SR. These results strongly suggest that the SRs are always more likely to move. In the next section, we have studied the kink migration for both the partials.

5. Kink migration analysis

The activation energy for long dislocation segments is the sum of the formation energy F_{k} of the single kink and the kink migration energy W_{m} in Hirth–Lothe theory [21]. The formation energy controls the density of kinks in thermodynamic equilibrium, while W_{m} determines the expansion of the kinks along the dislocation line. When the dislocation length is smaller than the mean

separation between kinks or strong obstacles, the activation energy becomes $Q = 2F_k + W_m$. The latter expression controls the migration velocity for short dislocation segments. Kinks can only be formed in pairs and the formation energy of a kink pair when the separation of the single kinks is $n \cdot b$ is defined by

$$2F_k = \triangle E_{\text{kinkpair}} + E_{\text{int}}(n) \tag{5}$$

where F_k is the formation of a single kink, $\triangle E_{\text{kinkpair}}$ is the formation energy of a kink pair with the smallest possible separation and the E_{int} is the kink–kink interaction term. The latter term is approximately given by elasticity theory [21]

$$E_{\text{int}}(n) = -\frac{\mu b_p^2 h^2}{8\pi n a_0}\frac{1-2\nu}{1+\nu} \simeq -\frac{0.24}{n}\,\text{eV}, \tag{6}$$

where μ is the shear modulus (1.23 eV Å^{-3} [22]), b_p is the modulus of the Burgers vector ($a_0/\sqrt{3}$), ν is Poisson's ratio (0.21 [23]), h is the height of the kink ($a/\sqrt{3}$) and $n \cdot a_0$ is the separation between single kinks ($a_0 = 3.06$ Å). The term $\triangle E_{\text{kinkpair}}$ is found by introducing a kink pair along the dislocation line for both the C(g) and Si(g) core dislocations. The formation energies are then found by subtracting the energies of the corresponding straight dislocations.

To model the single kink and kink pair, we have used a hybrid cluster–supercell approach, with several layers along the dislocation line (supercell component). The stoichiometry of the unit cells used is $Si_{35}C_{35}H_{24}$ per layer. Test calculations have shown that seven layers along the dislocation line are large enough to describe quantum-mechanically bonds and energies of the kinked dislocations. The so-built unit cells include two topologically equivalent kinks separated by 3–4 layers along the dislocation line.

Figure 4 shows the elementary step of single kink migration. The migrated kink is found by rotating the central Si(g) and C(g) atoms (arrows in figure 4) by about 90° along an axis normal to the glide plane. This causes a kink migration along the dislocation and a consequent expansion of the stacking fault region associated with the partials. To investigate the intermediate structures between the initial and migrated kink, we have defined two variables c_{silicon} and c_{carbon} associated with the two central atoms:

$$c_{\text{silicon}} = |R_1 - R_4|^2 - |R_1 - R_3|^2; \quad c_{\text{carbon}} = |R_2 - R_3|^2 - |R_2 - R_4|^2. \tag{7}$$

The atoms involved in the constraints are labelled in figure 4. In the case of the SR C(g) core dislocation only one atom (the silicon one) is mainly involved in the migration process, therefore only one constraint is used. Then meshes of 10×10 intermediate points were used to model the single kink migrations. For fixed values of the constraints c_{silicon} and c_{carbon} all the structures are relaxed using the conjugate gradient method. Figure 5 shows the two-dimensional energy surface for the kink migration of the C(g) core partial.

5.1. C(g) core dislocations

In the SR the distances between dangling bond atoms closest to the kink step are 2.83 Å, while the others far from the kink step reproduce the value of the straight dislocation (2.69 Å). The migration barrier W_m is found exactly at the origin of the constraint space with saddle point energy

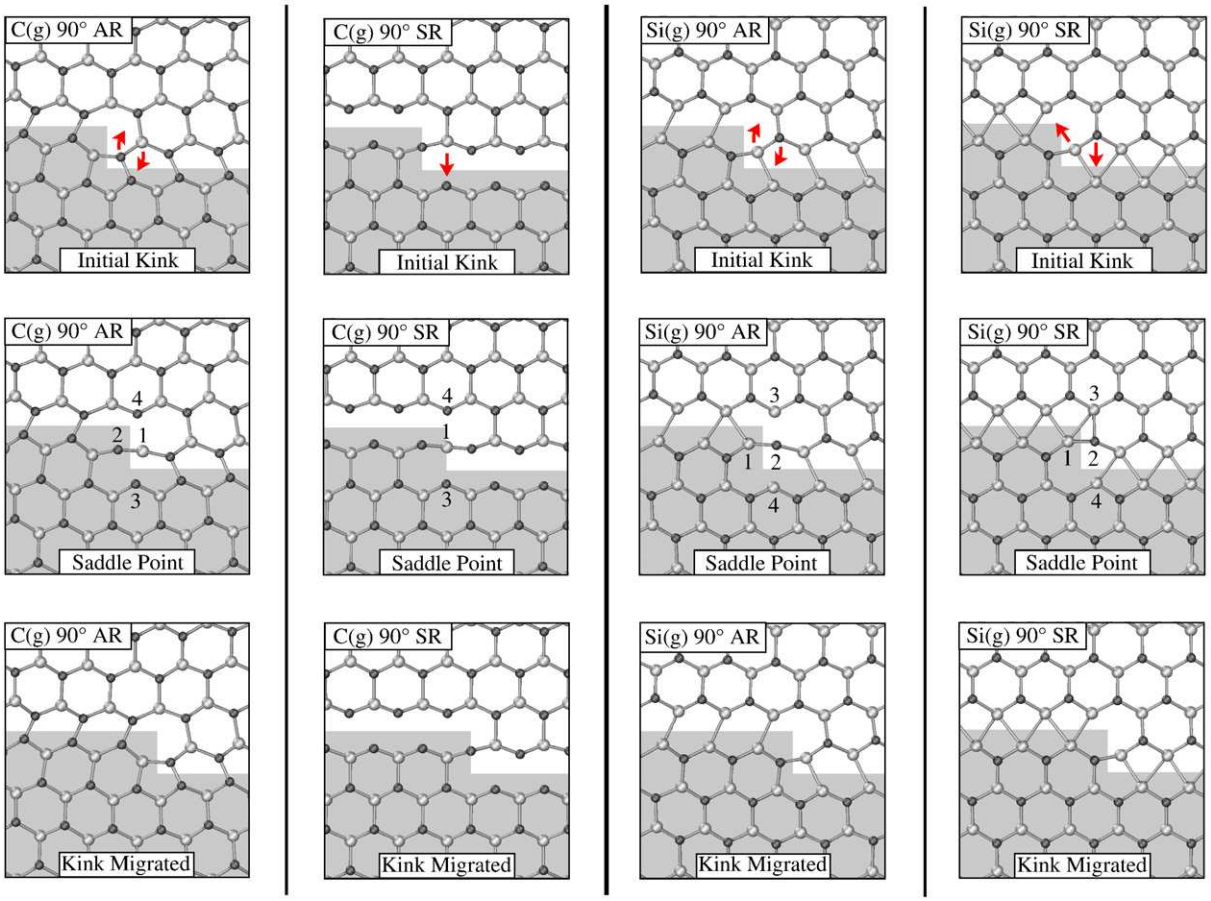

Figure 4. Kink migration for the C(g) core dislocation (first column: AR, second column: SR) and Si(g) core dislocation (third column: AR, fourth column: SR). (Top) initial kink. The arrowheads indicate the atoms mainly involved during the kink migrations. (Centre) saddle point. The numbers show the atom positions used by the constraints. (Bottom) kink migrated. The shaded regions underline the stacking fault expansion associated with the kink migrations.

of 0.21 eV. The formation energy $2F_k$ for the corresponding kink pair is 0.40 eV. Therefore the activation energy Q for the migration of short segment dislocations is 0.61 eV. In the AR the C–C bonds closest to the kink step are slightly compressed with lengths of 1.64 Å, while the others reproduce the bond length of the straight dislocation (1.65 Å). The back bonds range between 1.81–2.04 Å, representing strains of up to 9%. We have found a saddle point near the origin of the constraints c_{silicon}, c_{carbon} with migration energy W_m of 1.78 eV. The formation energy $2F_k$ for the corresponding kink pair is 0.36 eV. This yields an activation energy Q of 2.14 eV for short segment dislocations.

5.2. Si(g) core dislocations

For the SR, the lengths between dangling bond atoms close to the single kink are 2.57 Å (expanded by 8% with respect to the straight dislocation). The back bonds have lengths between 1.84–1.92 Å,

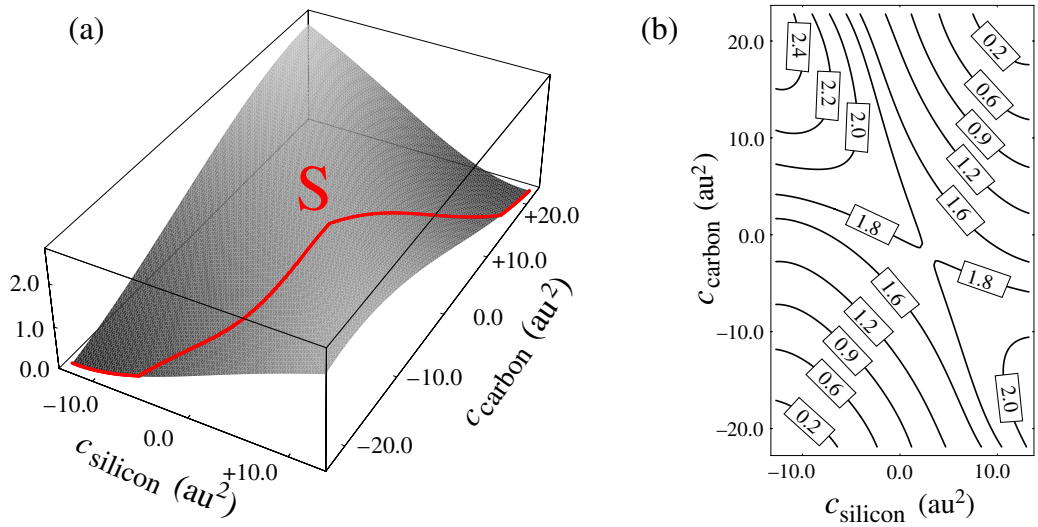

Figure 5. (a) Surface energy and (b) contour plot of the kink migration for the C(g) core dislocation. The two global minima represent the energy of the initial and migrated kink, while the maximum of the migration path (indicated with S) represents the saddle point.

Table 3. Kink pair formation energies $2F_k$ and migration barrier W_m for the 90° partial dislocations in the AR (neutral charge state) and SR (negative charge state). The resulting glide activation energies $Q = 2F_k + W_m$ are relevant for short segment dislocations. The numbers in brackets are the respective activation energies for long segment dislocations ($Q = F_k + W_m$).

	Core structure	$\triangle E_{kinkpair}$ (eV)	$2F_k$ (eV)	W_m (eV)	Q (eV)
C(g) core	AR (0 e)	0.12	0.36	1.78	2.14 (1.96)
	SR (−1 e)	0.16	0.40	0.21	0.61 (0.41)
Si(g) core	AR (0 e)	0.10	0.34	1.85	2.19 (2.02)
	SR (−1 e)	0.97	1.21	0.34	1.55 (0.95)

representing strains of up to 2%. The saddle point energy W_m is 0.34 eV, while the formation energy $2F_k$ is 1.21 eV. This yields the corresponding activation energy Q of 1.55 eV for short dislocation segments. In the AR, the Si–Si bonds closest to the kink step are 2.37 Å (only 0.4% compressed with respect to the straight dislocation) and 2.45 Å (3% stretched with respect to the straight dislocations). The back bonds have lengths ranging between 1.84–1.92 Å representing strains of up to 2% (exactly the same as the SR). The difference in energies between the kink pair and the straight dislocation is 0.10 eV and the corresponding formation energy $2F_k$ is 0.34 eV. The saddle point barrier for the kink migration is 1.85 eV which gives an activation energy Q of 2.19 eV for short dislocation segments.

The respective formation energies $2F_k$, migration barrier W_m and activation energies Q are summarized in table 3. For both the partials, the dislocation dynamics of the ARs are controlled by the kink migration barrier W_m ($W_m > 2F_k$), while for the SRs the dislocation dynamics are governed by the kink formation energy $2F_k$ ($2F_k > W_m$).

6. Conclusions

First-principles calculations showed that both the Si(g) and C(g) dislocations can support the SRs and ARs. In the AR only the Si(g) core dislocations are electrically active with an energy level of $E_v + 0.2$, in agreement with a previous study [11]. In strongly n-type materials, the SR, characterized by dangling bonds along the dislocation line, can become favourable. These reconstructions are always electrically active, the C(g) core dislocations give rise to a deep band ranging from the top of the VB to $E_v + 1.97$, while the Si(g) core dislocations give rise to a deep band ranging from $E_v + 0.21$ eV to the top of the CB.

The kink migration analysis showed that SR is always more likely to move. For the C(g) core partial, the activation energy Q is lowered from 2.14 eV for the AR to 0.61 eV for the SR, while for the Si(g) core the activation energy Q is lowered from 2.19 eV for the AR to 1.55 eV for the SR. The higher activation energy of the SR Si(g) core reflects the stronger core reconstruction of the quasi 5-fold coordinate atoms along the dislocation line (see figure 1(d)). The Peierls barriers of the first kind confirm the kink migration results within a range of ∼30%. The fairly good agreement suggested an alternative method to calculate the glide activation energies in a more approximate way (but computationally far less expensive) than the full kink migration analysis.

Our results have shown that the AR does not possess band-gap levels deep enough, as required by the REDG mechanism and have large activation barriers preventing motion at room temperature. However the SRs are always electrically active, with bands deep enough as required by REDG mechanism. The migration energy of the SRs are dramatically reduced compared with the respective ARs and could be further reduced by the REDG mechanism.

We suggest that under forward bias, the free energy of the SRs can be dynamically lowered by continuous electron–hole transitions between the respective deep levels and VBs/CBs. This suggestion could explain why under electron–hole plasma injections the dislocations easily glide in both n-type and p-type materials [4, 24].

However, we have shown that the SR of the 90° partials requires a shear between the unfaulted and stacking fault regions along the dislocation line of the AR, while for the 30° partials the SR should not require a long ranged shear, but rather only requires flipping of alternate atoms in the core [25, 26]. Therefore we suggest that under forward bias only the 30° partials become symmetrically reconstructed allowing motion at room temperature, while the 90° partials are always locked by the ARs. Nevertheless at high temperature and with low electron-hole carrier injections the 90° partials are the more mobile species with the C(g) core slightly faster than the Si(g) core ($Q = 1.71$–2.01 eV for the 90° partials and $Q = 4.6$–5.0 eV for the 30° partials [11]).

The good agreement in atomic structures, electrical properties and activation energies between different polytypes (4H–SiC in the present study, 2H- and 3C–SiC in [11]) indicates that the partial dislocations are topologically equivalent regardless of the different polytypes. This is especially true among the hexagonal types which possess nearly identical values of forbidden band-gap $\Delta E_g \sim 2.9$–3.3 eV [1] and almost identical elastic constants [11]. However, our results have shown that the SRs become more favourable than the AR ones only with a Fermi energy E_F larger than ∼2.9 eV (see figure 2(a) and (b)). Due to the smaller forbidden band-gap $\Delta E_g = 2.3$ eV, the latter requirement is less probable in 3C–SiC. Therefore our study suggests that in cubic polytypes the dislocations are more likely asymmetrically reconstructed, i.e. they possess higher glide activation energies and they are less electrically active compared

with hexagonal polytype. Recently Speer *et al* [27] have reported the first preliminary evidence of dislocation motion absence in 3C–SiC by electron channelling contrast imaging.

Acknowledgments

We thank the UK high performance computing (HPC) and the Swedish National Research Council (SNIC). Gianluca Savini thanks the Programma Marco Polo for financial support and the High End Computing Strategy Committee for the HPC Prize 2006.

References

[1] Morko H, Strite S, Gao G B, Lin M E, Sverdlov B and Burns M 1994 *J. Appl. Phys.* **76** 1363
[2] Bergman J P, Lendenmann H, Nilsson P Å, Lindefelt U and Skytt P 2001 *Mater. Sci. Forum* **299** 353
[3] Galeckas A, Linnros J and Pirouz P 2002 *Appl. Phys. Lett.* **81** 883
[4] Ha S, Skowronski M, Sumerakis J J, Paisley M J and Das M K 2004 *Phys. Rev. Lett.* **92** 175504
[5] Ha S, Benamara M, Skowronski M and Lendenmann H 2003 *Appl. Phys. Lett.* **83** 4957
[6] Skowronski M, Liu J Q, Vetter W M, Dudley M, Hallin C and Lendenmann H 2002 *J. Appl. Phys.* **92** 4699
[7] Twigg M E, Stahlbush R E, Fatemi M, Arthur S D, Fedison J B, Tucker J B and Wang S 2003 *Appl. Phys. Lett.* **82** 2410
[8] Weeks J D, Tully J C and Kimerling L C 1975 *Phys. Rev.* B **12** 3286
[9] Sumi H 1984 *Phys. Rev.* B **29** 4616
[10] Maeda K and Takeuchi S 1996 *Dislocation in Solids* vol 10, ed F R N Nabarro and M S Duesbery (Amsterdam: North-Holland) pp 443–504
[11] Blumenau A T, Fall C J, Jones R, Öberg S, Frauenheim T and Briddon P R 2003 *Phys. Rev.* B **68** 174108
[12] Skowronski M and Ha S 2006 *J. Appl. Phys.* **99** 011101
[13] Perdew J P and Wang Y 1992 *Phys. Rev.* B **45** 13244
[14] Briddon P R and Jones R 2000 *Phys. Status Solidi* B **217** 131
[15] Hartwigsen C, Goedecker S and Hutter J 1998 *Phys. Rev.* B **58** 3641
[16] Monkhorst H J and Pack J D 1976 *Phys. Rev.* B **13** 5188
[17] De Arajo M M, Justo J F and Nunes R W 2004 *Appl. Phys. Lett.* **85** 5610
[18] Laks D B, Van de Walle C G, Neumark G F, Blöchl P E and Pantelides S T 1992 *Phys. Rev.* B **45** 10965
[19] Suzuki T and Takeuchi S 2000 *Crystal Lattice Defects and Dislocation Dynamic* ed R A Vardanian (New York: Huntington) pp 1–66
[20] Peierls R E 1940 *Proc. Phys. Soc.* **52** 34
[21] Hirth J P and Lothe J 1982 *Theory of Dislocations* 2nd edn (New York: Wiley) p 244
[22] Amulele G M, Manghnani M H, Li B, Errandonea D J H, Somayazulu M and Meng Y 2004 *J. Appl. Phys.* **95** 1806
[23] Karmann S, Helbig R and Stein R A 1989 *J. Appl. Phys.* **66** 3922
[24] Galeckas A, Linnros J and Pirouz P 2006 *Phys. Rev. Lett.* **96** 025502
[25] Bernardini F and Colombo L 2005 *Phys. Rev.* B **72** 085215
[26] Savini G, Heggie M I and Öberg S 2006 *Mater. Sci. Forum* **527-529** 359
[27] Speer K M, Spry D J, Trunek A J, Neudeck P G, Crimp M A, Hile J T, Burda C and Pirouz P 2007 *Mater. Sci. Forum* in press